Electronic Supplementary Information

Metal Organic Framework (MOF)-5/CuO@$ZnIn_2S_4$ Core-Shell Z-Scheme Tandem Heterojunctions for Improved Charge Separation and Enhanced Photocatalytic Performance

Yi Yang[a], Zipeng Xing[a, *], Weifeng Kong[a], Chunxu Wu[a], Hui Peng,[a] Zhenzi Li[b, *], Wei Zhou [a,b, *]

[a] Department of Environmental Science, School of Chemistry and Materials Science, Key Laboratory of Functional Inorganic Material Chemistry, Ministry of Education of the People's Republic of China, Heilongjiang University, Harbin 150080, P. R. China

Tel: +86-451-8660-8616, Fax: +86-451-8660-8240,

Email: xingzipeng@hlju.edu.cn; zwchem@hotmail.com

[b] Shandong Provincial Key Laboratory of Molecular Engineering, School of Chemistry and Chemical Engineering, Qilu University of Technology (Shandong Academy of Sciences), Jinan 250353, P. R. China

Email: zhenzhenlee2014@163.com

Experimental section

Materials

Anhydrous ethanol (EtOH) and N,N-dimethylformamide (DMF) were purchased from Tianjin Kemer Chemical Reagent Co. Zinc nitrate hexahydrate ($ZnNO_3 \cdot 6H_2O$), terephthalic acid (PTA), polyvinylpyrrolidone (PVP), zinc chloride ($ZnCl_2$), indium trichloride tetrahydrate ($InCl_3 \cdot 4H_2O$), thioacetamide (TAA), and copper nitrate tetrahydrate ($CuNO_3 \cdot 4H_2O$) were purchased from Aladdin Industrial. Glycerol (GE) was purchased from Tianjin Guangfu Science and Technology Development Co. 2,4-dichlorophenol (2,4-DCP), phenol, methyl orange (MO) and methylene blue (MB) were all purchased from Tianjin Kemiou Chemical Reagent Company. All chemicals were analytic reagents and used as received. The deionized water was used throughout this study.

Characterizations

X-ray diffraction (XRD) was obtained by a Bruker D8 Advance diffractometer (using Cu Kα radiation, λ = 1.54056 Å, 40 kV, 40 mA). Scanning electron micros-copy (SEM) images were obtained with a Philips XL-30-ESEM-FEG instrument operating at 20 kV. Transmission electron microscope (TEM) JEOL JEM-2010 at an accelerating voltage of 200 kV was also used to record the electron micrographs of the samples. X-ray photoelectron spectroscopy (XPS, Kratos, ULTRA AXIS DLD) was carried out with monochrome Al Kα ($h\nu$ = 1486.6 eV) radiation. UV-vis diffuse reflection spectra (DRS) were recorded on a UV-vis spectrophotometer (UV-2550, Shimadzu) with an integrating sphere attachment, and $BaSO_4$ was used as the reference material. The ·OH

radicals and $\cdot O_2^-$ radicals were detected by the fluorescence probe technique with coumarin on a RF-5301PC fluorescence spectrophotometer and a 300 W Xenon lamp. Surface area was estimated by BET method and pore-size distribution was measured from the adsorption branch of the isotherm using the Barrett-Joyner-Halenda (BJH) method. The photoluminescence (PL) spectra were measured with a PE LS 55 spectrofluorophotometer at excitation wavelength of 400 nm. The work function of samples was tested by Scanning Kelvin probe (SKP) (SKP5050 system, Scotland). The temperature of the sample was measured using the Testo 865 infrared thermograph. Incident photon-to-current efficiency (IPCE) measurements were using the Newport 2936-C in a standard three electrode configurations with catalytic used as photoanodes, Pt foil as the counter electrode, and Ag/AgCl ($E_{Ag/AgCl}$ is 0.6 eV vs. NHE) reference electrode in home-built crystal equipment containing 1 M KOH solution. The electron spin resonance (ESR) spectra under visible light irradiation were tested with ESR spectrometer (Bruker model A300). The temperature of the sample was measured using the Testo 865 infrared thermograph.

Photocatalytic degradation activity tests

Important pharmaceutical intermediates such as 2,4-DCP and phenol, as well as dyes such as methyl orange and methyl blue, were selected to test the photocatalytic degradation performance. The experiments were carried out in winter in Harbin (44°04′ N, 125°42′ E) and the room temperature was maintained at 12±2°C. In a typical experiment, photocatalyst (30 mg) was added to MO solution (30 mL, 10 mg/L), MB solution (30 mL, 10 mg/L), phenol solution (30 ml, 10 mg l), and 2,4-DCP solution (30

mL, 10 mg/L). The suspensions were then placed in the dark to ensure adsorption-desorption equilibrium. 300 W xenon lamps were used to irradiate the suspensions and the residual MO, MB, phenol or 2,4-DCP concentrations were analyzed using a T6 UV-Vis spectrophotometer.

Photocatalytic hydrogen evolution

The photocatalytic H_2 evolution experiments were conducted in an online hydrogen generation system. During the photocatalytic hydrogen evolution reaction, the samples (100 mg) were dispersed in 100 mL of methanol/H_2O solution ($V_{methaol}$: V_{H2O} = 1:4). Before light irradiation, the reactor and the entire gas circulating system were fully degassed to remove air using a vacuum pump for 30 min. Before the photoreactions, the dispersion was sonicated for 10 min. A 300 W Xe lamp was used as the light source that simulated the full-spectrum source. The photocatalytic H_2 evolution was analyzed using a gas chromatograph (SP7800, TCD, molecular sieves 5 Å, N_2 carrier, Beijing Keruida Limited).

Photothermal and photoelectrochemical measurements

The electrochemical impedance spectroscopy and photocurrents curves were examined by the Princeton workstation, which employed the three-electrode configuration. Na_2S (0.1 M) aqueous solution was used as the electrolyte solution. Pt foil was the counter electrode and Ag/AgCl electrode was used as the reference electrode. In order to prepare working electrode, photocatalyst sample (50 mg) was dispersed in ethanol (35 mL), and then the suspension was sprayed onto the FTO glass, and then the FTO glass was calcined at 200 °C for 2 h in Ar. Furthermore, a 300 W

Xenon lamp was used as the light source. Electro-chemical impedance spectroscopy was measured with amplitude of 5 mV and frequencies varying from 0.01 to 10000 Hz.

The photothermal test of as-prepared samples was carried out as follow. 0.1 g of samples was loaded on a white paper and the initial temperature was controlled at room temperature. The temperature of the sample was measured using the Testo 865 infrared thermograph. A 300 W Xenon lamp was used as a light source.

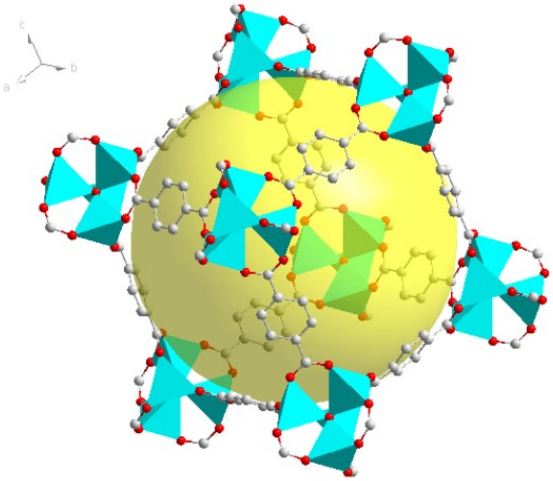

Figure S1. Schematic diagram of the crystal structure of MOF-5. (Cyan represents Zn atoms, red represents O atoms, and gray represents C atoms, with H atoms removed for clarity.)

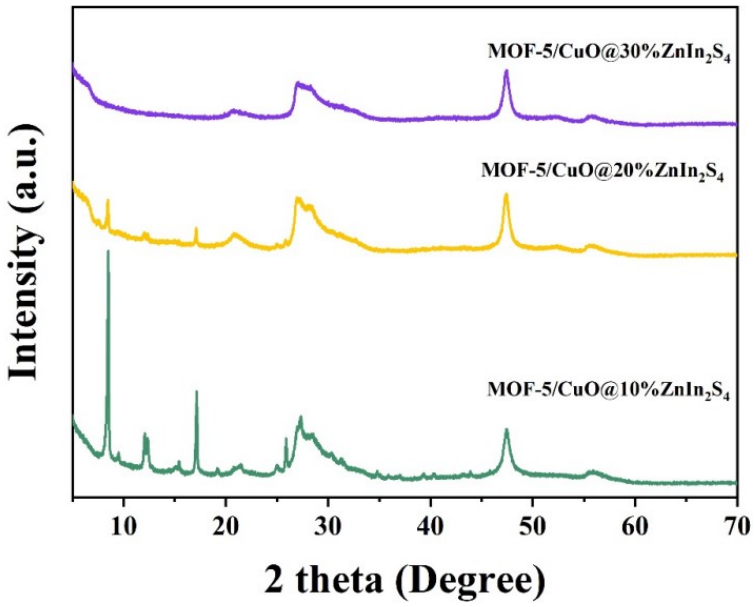

Figure S2. The XRD patterns of MOF-5/CuO@10% $ZnIn_2S_4$, MOF-5/CuO@20% $ZnIn_2S_4$ and MOF-5/CuO@30% $ZnIn_2S_4$, respectively.

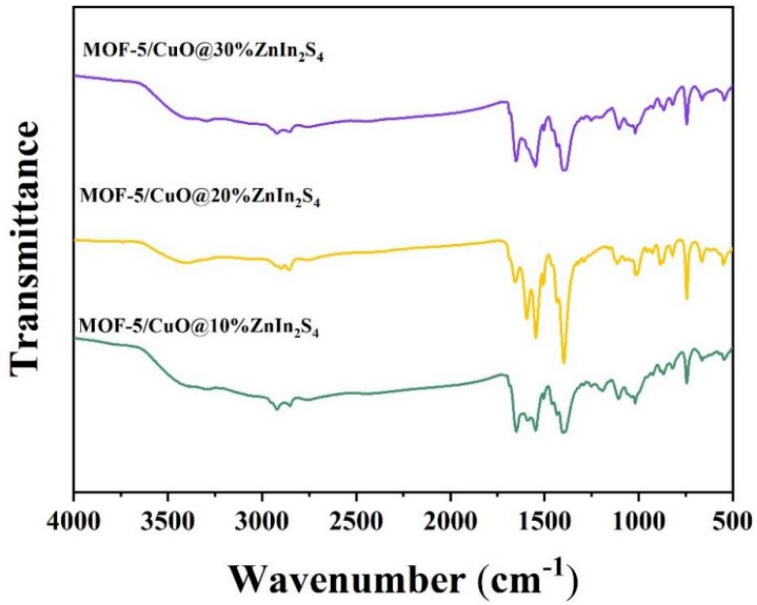

Figure S3. The FR-IT spectra of MOF-5/CuO@10% $ZnIn_2S_4$, MOF-5/CuO@20% $ZnIn_2S_4$ and MOF-5/CuO@30% $ZnIn_2S_4$, respectively.

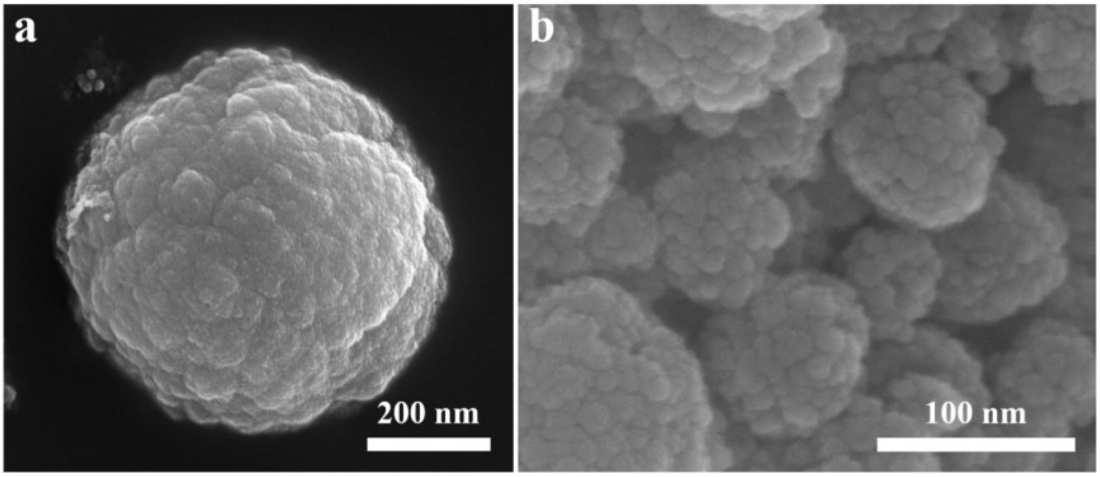

Figure S4. SEM images (a, b) of MOF-5 at different shooting sizes.

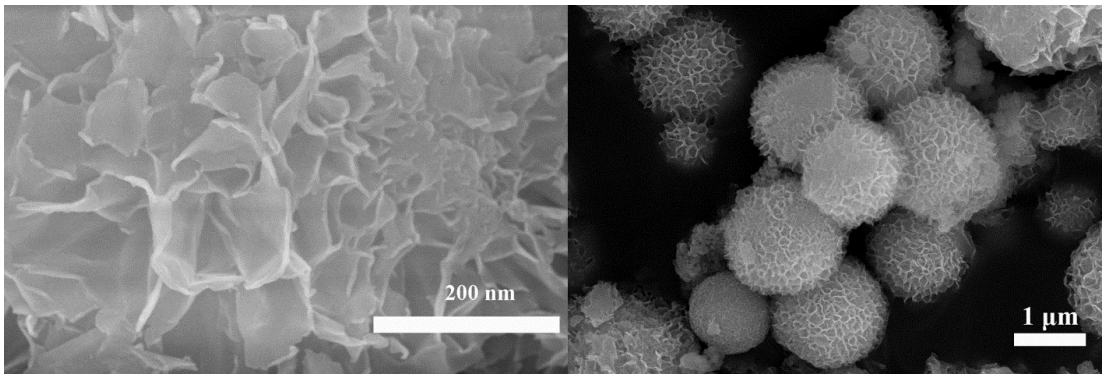

Figure S5. The SEM images of the individually grown $ZnIn_2S_4$.

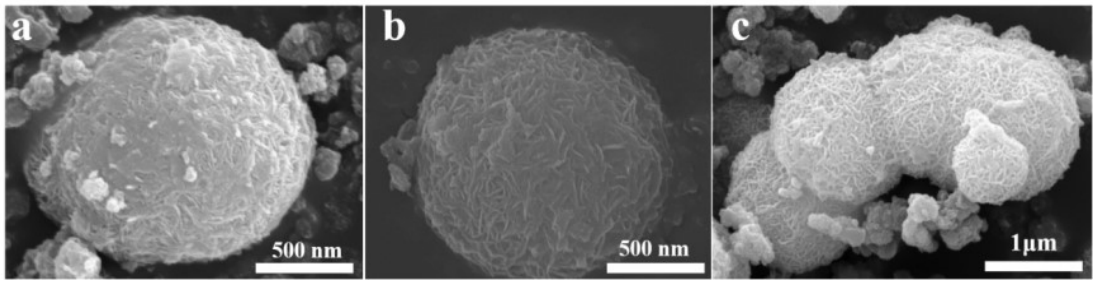

Figure S6. The SEM images of MOF-5/CuO@10% $ZnIn_2S_4$ (a), MOF-5/CuO@20% $ZnIn_2S_4$ (b), MOF-5/CuO@30% $ZnIn_2S_4$ (c), respectively.

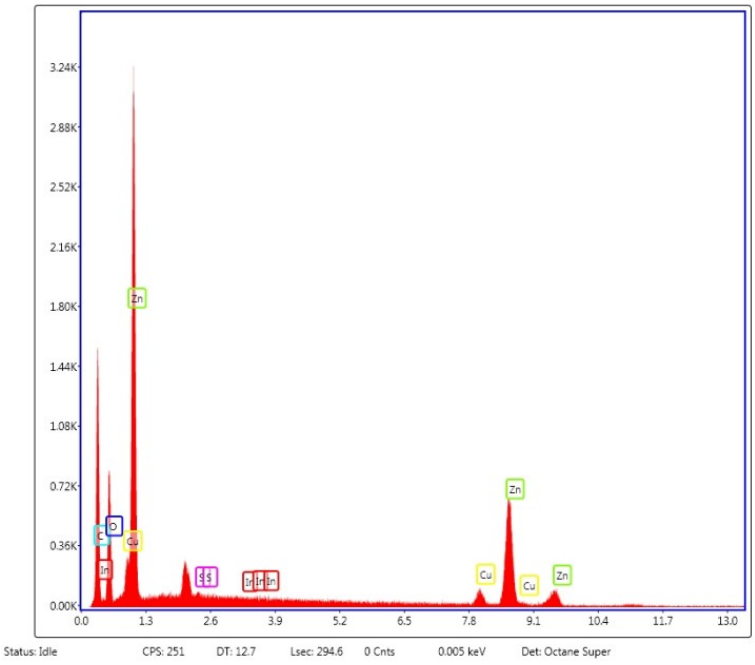

Figure S7. EDX elemental spectrum of MOF-5/CuO@$ZnIn_2S_4$.

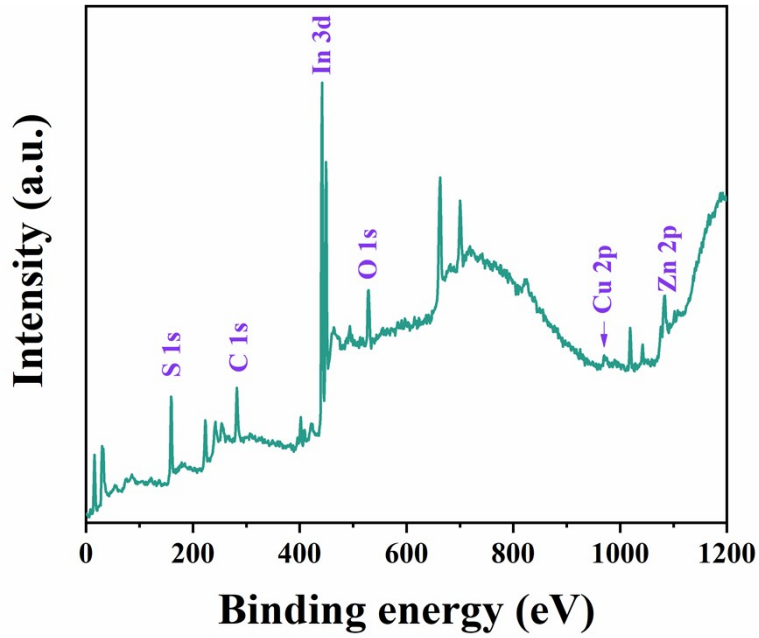

Figure S8. XPS survey spectrum of MOF-5/CuO@$ZnIn_2S_4$.

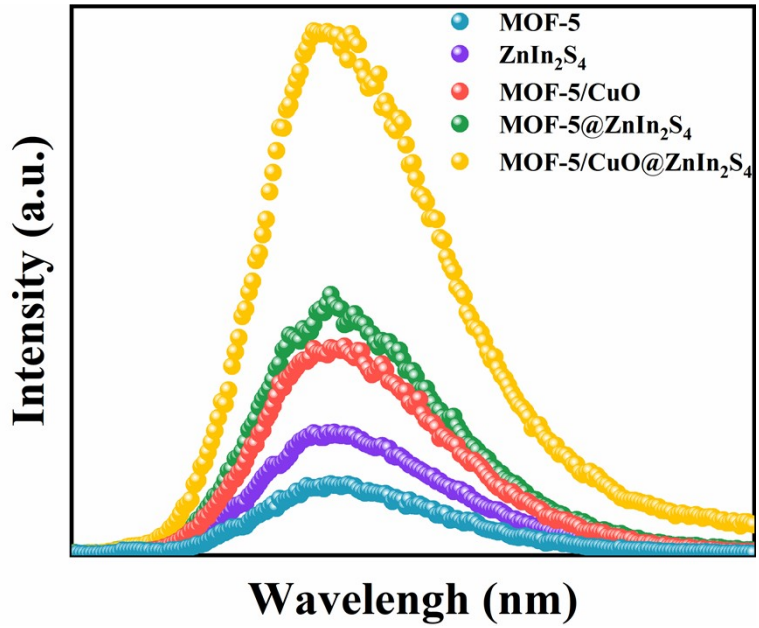

Figure S9. Fluorescence spectra of the as-prepared samples.

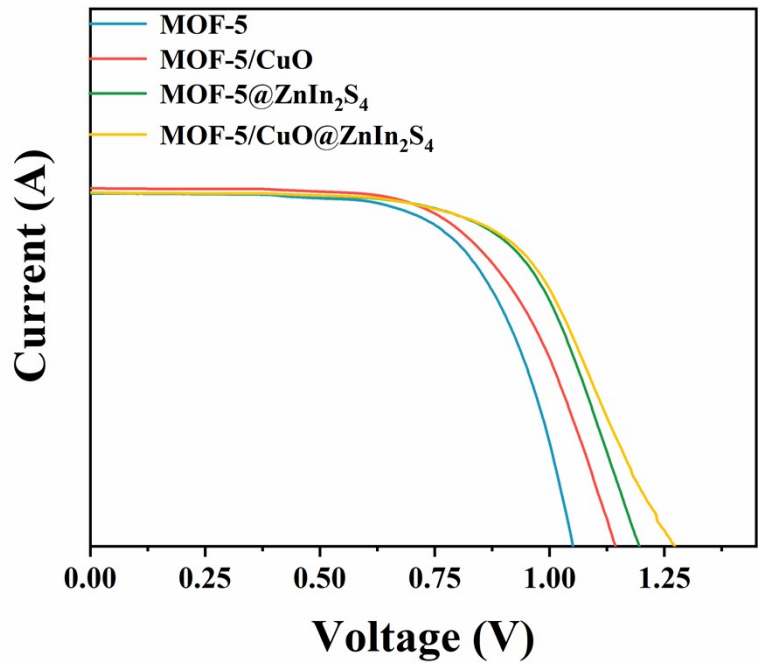

Figure S10. Solid-state current-voltage (I-V) curves of prepared photocatalysts.

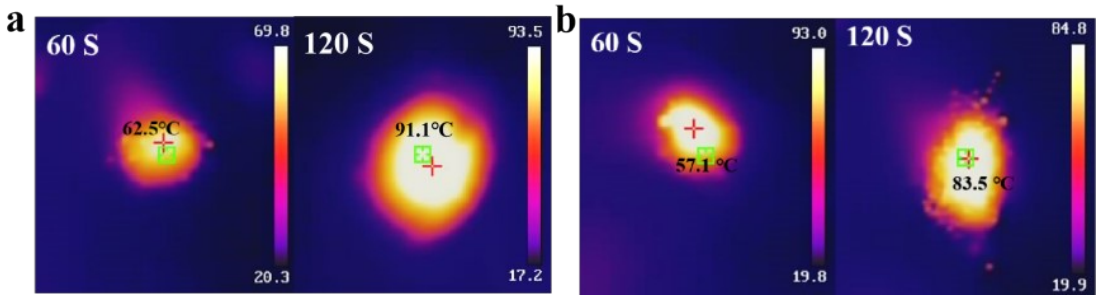

Figure S11. Infrared photographs of MOF-5/CuO (a) and MOF-5@$ZnIn_2S_4$ (b) with an onset temperature of 25 °C and 120 s of simulated solar irradiation.

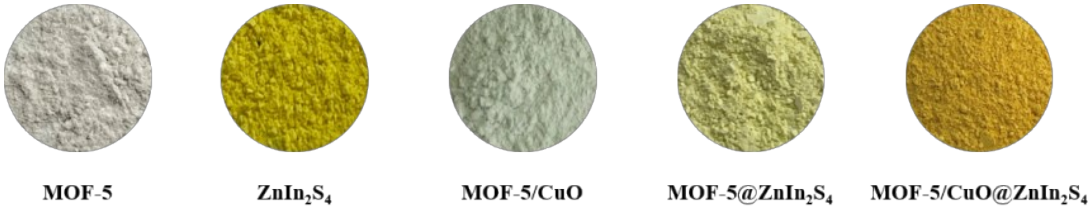

Figure S12. Digital photos of MOF-5, $ZnIn_2S_4$, MOF-5/CuO, MOF-5@$ZnIn_2S_4$, MOF-5/CuO@$ZnIn_2S_4$, respectively.

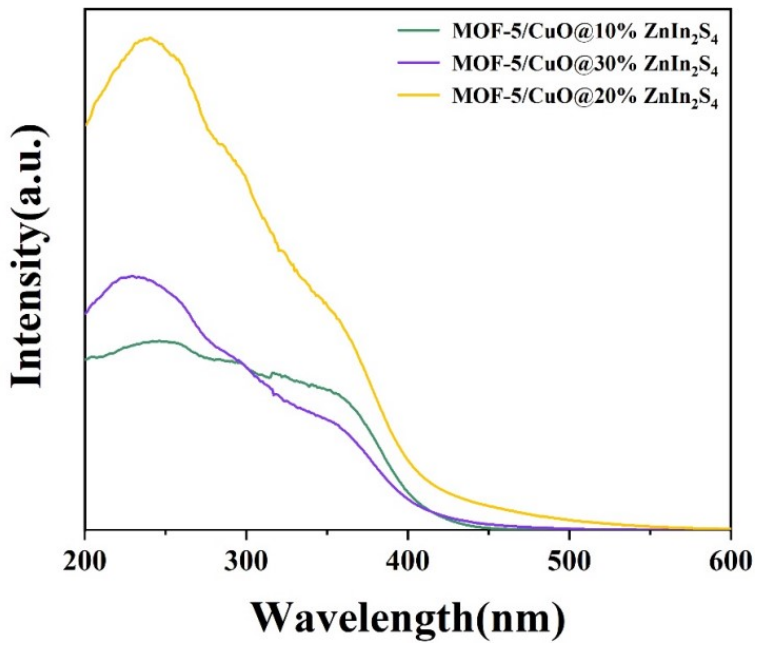

Figure S13. The UV-vis spectra of MOF-5/CuO@10% $ZnIn_2S_4$, MOF-5/CuO@20% $ZnIn_2S_4$ and MOF-5/CuO@30% $ZnIn_2S_4$, respectively.

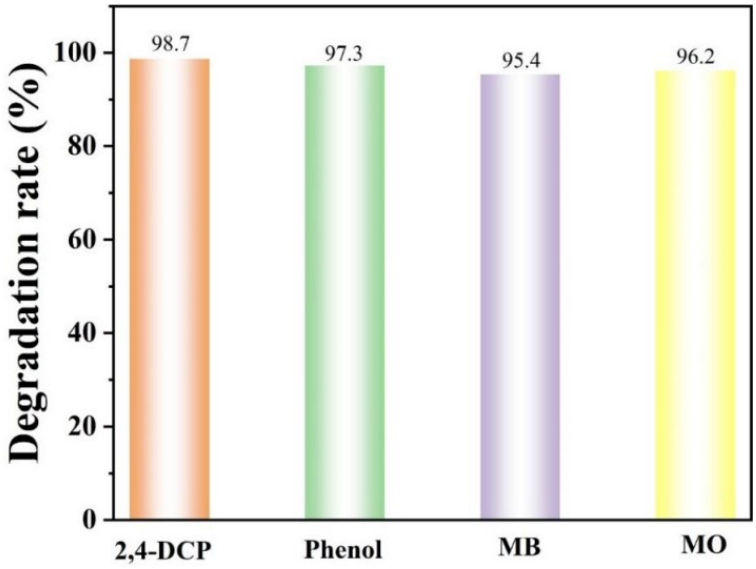

Figure S14. Photocatalytic degradation rates of MOF-5/CuO@$ZnIn_2S_4$ for different pollutants.

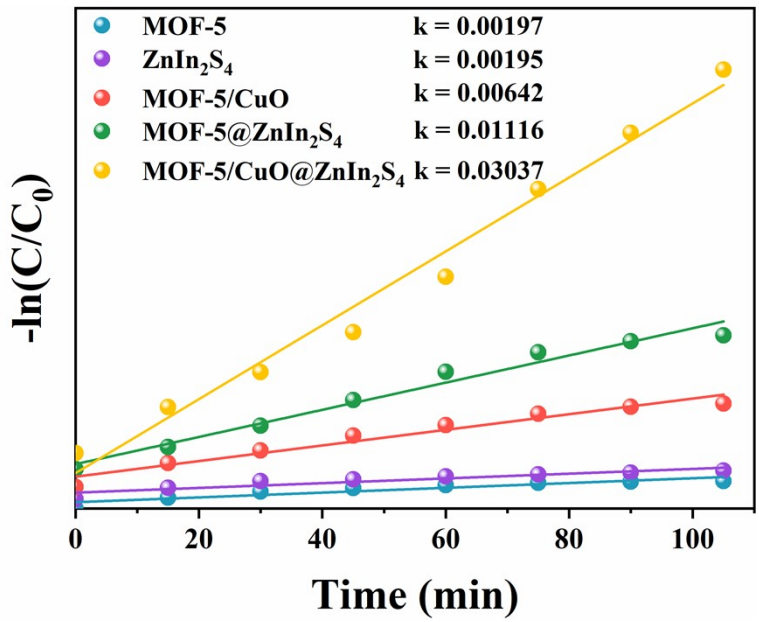

Figure S15. Pseudo primary kinetic plots of 2,4-DCP degradation by different photocatalysts under visible light irradiation.

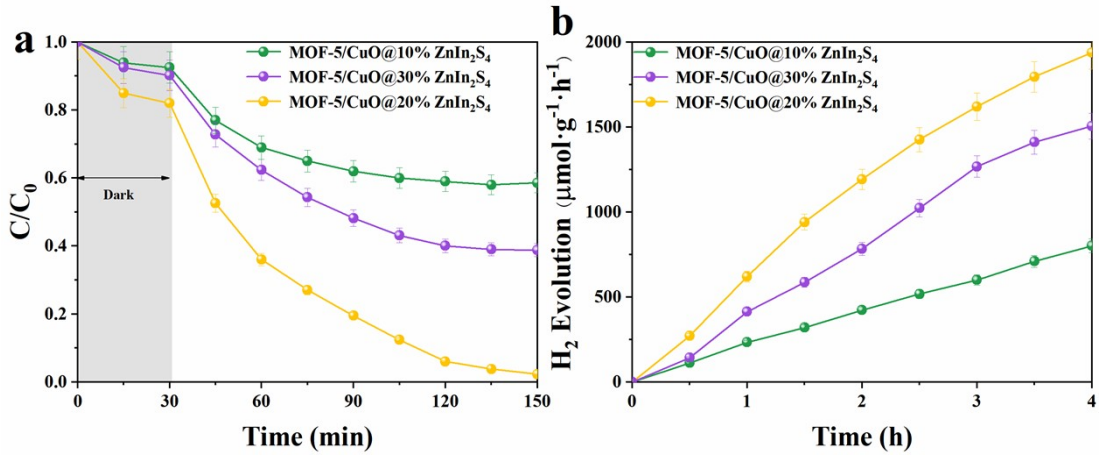

Figure S16. Photocatalytic degradation curves (a) and hydrogen evolution efficiency (b) of MOF-5/CuO@10%$ZnIn_2S_4$, MOF-5/CuO@20%$ZnIn_2S_4$ and MOF-5/CuO@30%$ZnIn_2S_4$, respectively.

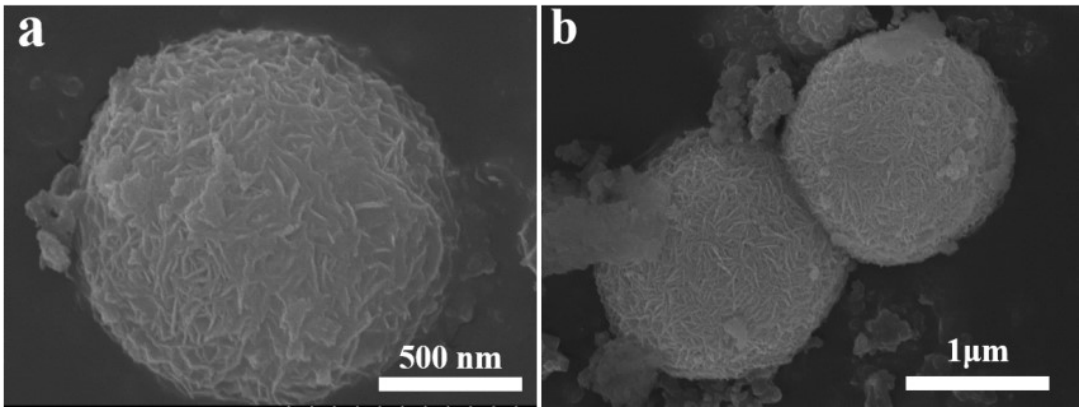

Figure S17. SEM images of MOF-5/CuO@$ZnIn_2S_4$ before (a) and after photocatalytic reaction (b).

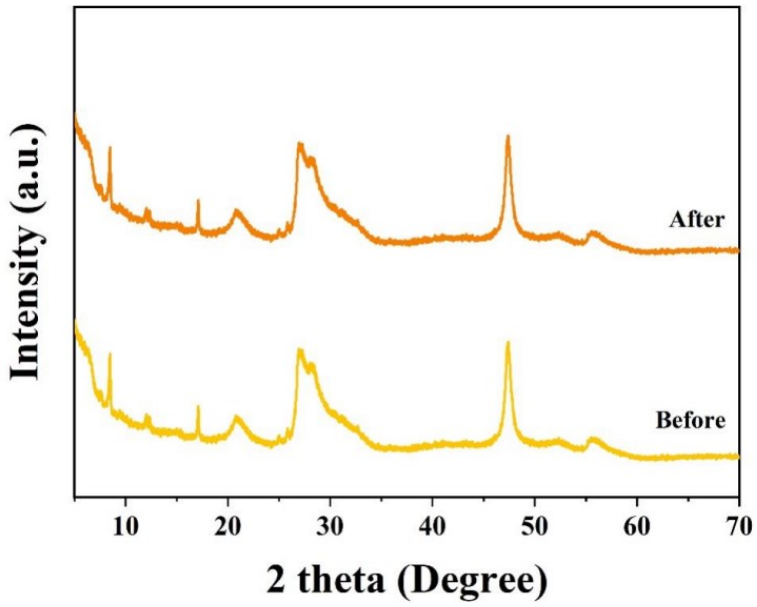

Figure S18. XRD patterns of MOF-5/CuO@$ZnIn_2S_4$ before and after photocatalytic reaction.

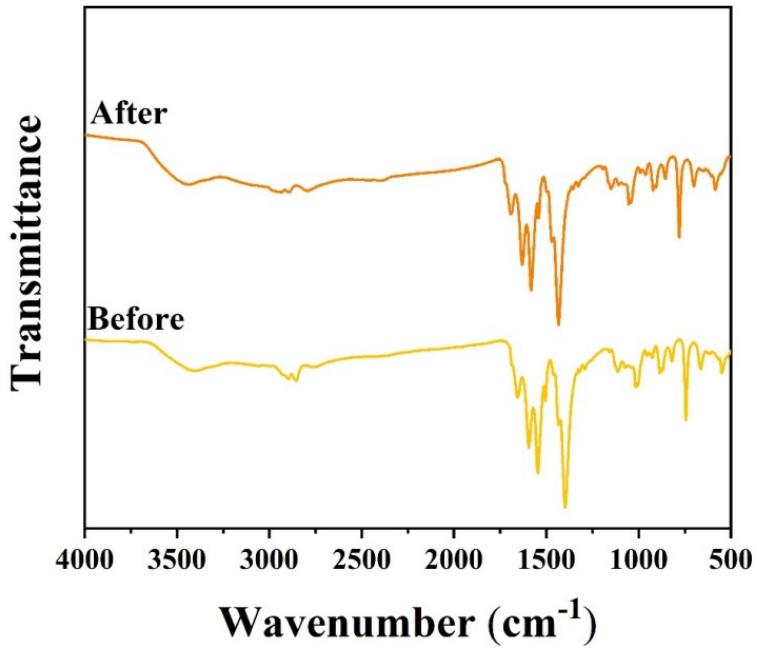

Figure S19. FR-IT spectra of MOF-5/CuO@$ZnIn_2S_4$ before and after photocatalytic reaction.

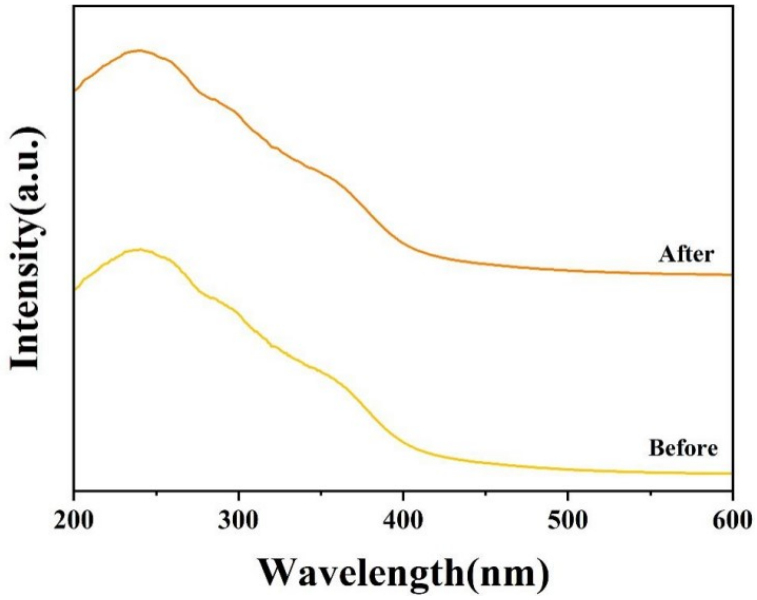

Figure S20. UV-Vis spectra of MOF-5/CuO@$ZnIn_2S_4$ before and after photocatalytic reaction.

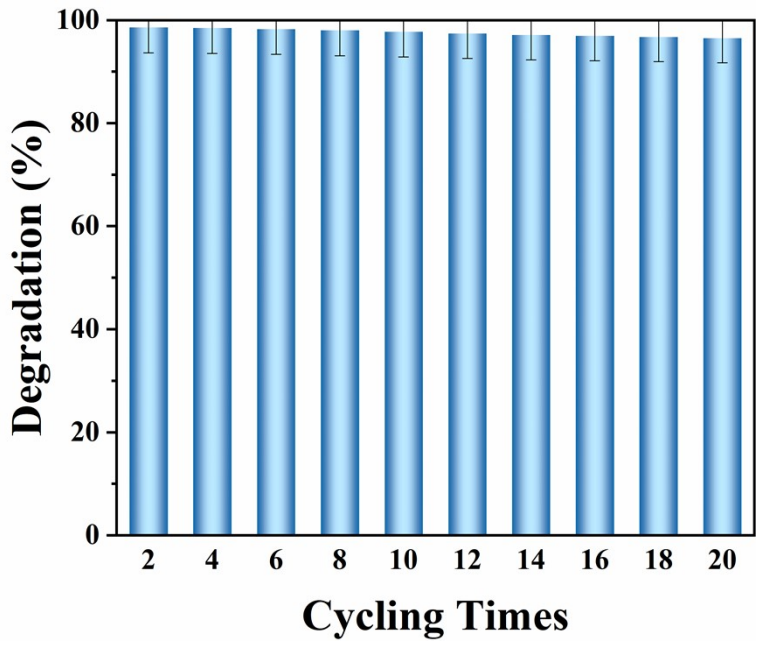

Figure S21. Long-term stability test experiment diagram of photocatalytic degradation of 2,4-DCP (20 cycles, 40 h).

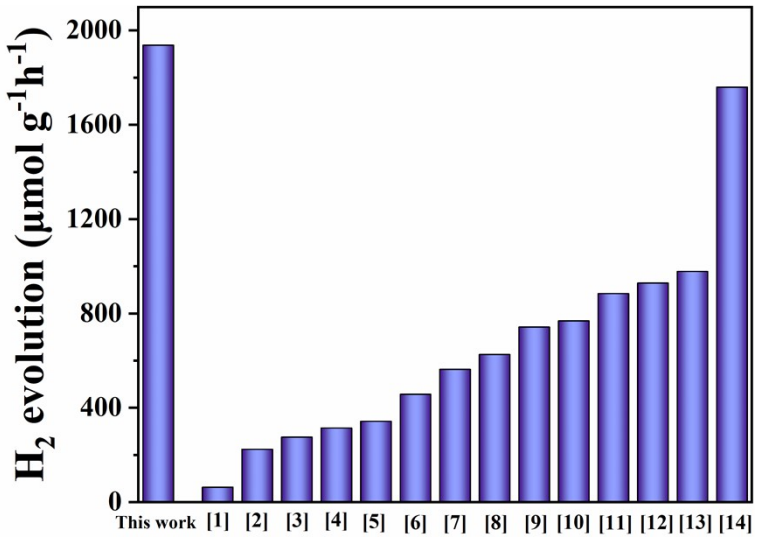

Figure. S22. The photocatalytic H_2 evolution rates of different photocatalysts.

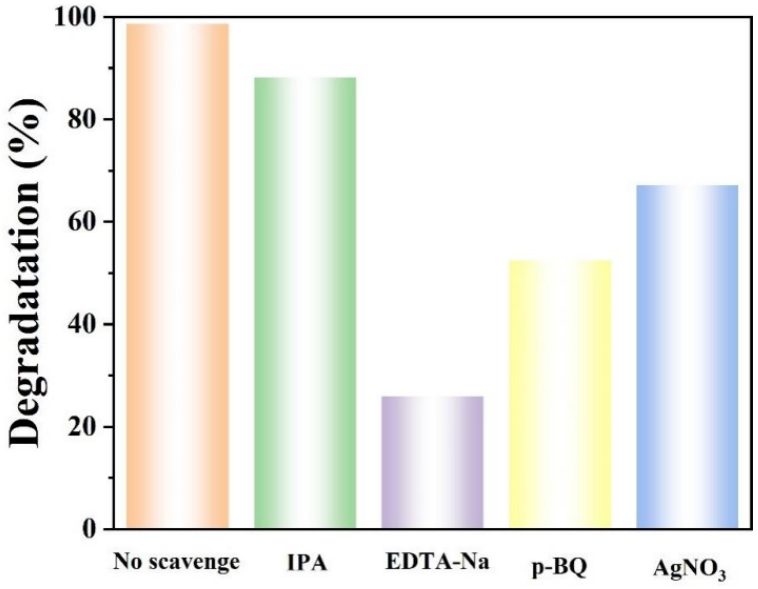

Figure S23. The species trapping experiments for photocatalytic degradation 2,4-DCP on MOF-5/CuO@$ZnIn_2S_4$.

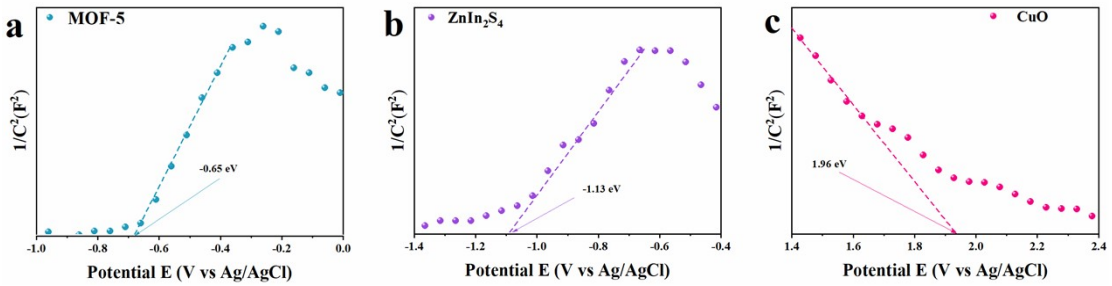

Figure S24. The Mott-Schottky plots of MOF-5 (a), $ZnIn_2S_4$ (b), CuO (c), respectively.

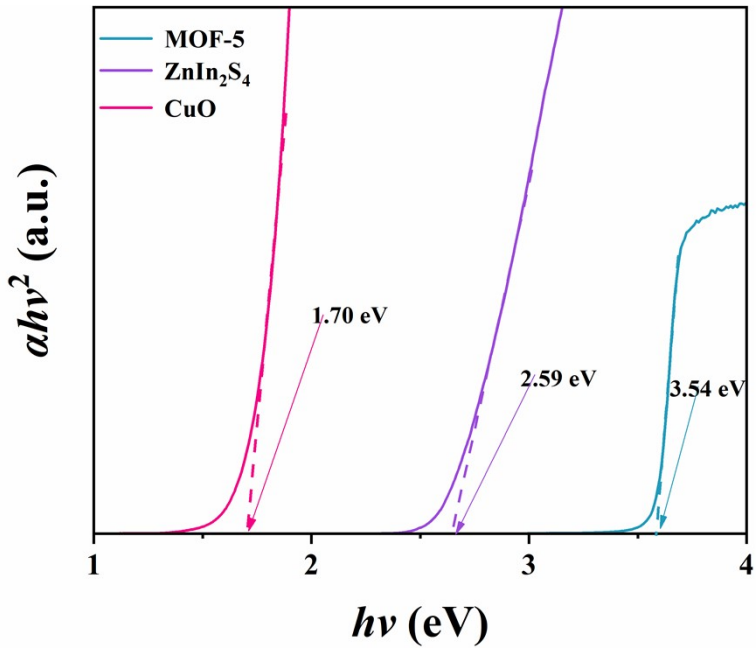

Figure S25. The corresponding optical bandgaps $(\alpha hv)^2$ versus hv curves for different samples.

Table S1. The specific BET surface areas of the as-prepared samples.

Photocatalyst	MOF-5	MOF-5/CuO	MOF-5@$ZnIn_2S_4$	MOF-5/CuO@$ZnIn_2S_4$
S_{BET} (m^2/g)	706.96	271.76	222.51	462.33

Table S2. The photocatalytic H_2 evolution rates of different photocatalysts.

Photocatalyst	**Rate of H_2 generation ($\mu mol \cdot g^{-1} \cdot h^{-1}$)**	**Sacrificial agent**	**ref**
$CdS@Ti_3C_2$	63.53	Triethanolamine (TEOA)	[1]
CdS/MoC	224.5	Lactic acid	[2]
$CeO_2/ZnIn_2S_4$	276	0.5M Na_2SO_3, Na_2S	[3]
EY-MIL-53(Fe)	315	TEOA	[4]
$MoS_2/ZnIn_2S_4$	343	Lactic acid	[5]
$CuO/CdS/CoWO_4$	457.9	Na_2SO_3, Na_2S	[6]
$BiVO_4$/RGO/CdS	563.7	Lactic acid	[7]
MOF-199/MoS_2	626.3	Formic acids	[8]
[Zn(L1)(L2)]	743	Na_2SO_3, Na_2S	[9]
$SnS_2/ZnIn_2S_4$	769	Lactic acid	[10]
$Cu_7S_4/ZnIn_2S_4$	885	Na_2SO_3, Na_2S	[11]
$MoOS_x$/CdS	929.4	Lactic acid	[12]
$ZnIn_2S_4/Ti_3C_2$	978.7	TEOA	[13]
$Cu_3(HHTP)_2$-MOF/Tp-Pa-1-COF	1760	Sodium ascorbate (SA)	[14]
MOF-5/CuO@$ZnIn_2S_4$	**1938.3**	**0.1 M Na_2SO_3, Na_2S**	**This work**

Table S3. The band gap energies, conduction band (CB) and valence band (VB) potentials (NHE) for MOF-5, CuO, and $ZnIn_2S_4$.

Photocatalyst	Band gap (eV)	CB (eV)	VB (eV)
MOF-5	3.54	-0.45	3.09
CuO	1.70	0.46	2.16
$ZnIn_2S_4$	2.59	-0.93	1.66

References

1 B. Sun, P. Qiu, Z. Liang, Y. Xue, X. Zhang, L. Yang, H. Cui, J. Tian, *Chem. Eng. J*, 2021, **406**, 127177.

2 Y. Lei, X. Wu, S. Li, J. Huang, K.H. Ng, Y. Lai, *J. Clean. Prod.*, 2021, **322**, 129018.

3 C. Zhu, Q. He, W. Wang, F. Du, F. Yang, C. Chen, C. Wang, S. Wang, X. Duan, *J. Colloid Interface Sci.*, 2022, **620**, 253-262.

4 S. Li, F. Wu, R. Lin, J. Wang, C. Li, Z. Li, J. Jiang and Y. Xiong, *Chem. Eng. J*, 2022, **429**, 132217.

5 B. Chai, C. Liu, C. Wang, J. Yan, Z. Ren, *Chinese J. Catal.*, 2017, **38**, 2067-2075.

6 N. Güy, K. Atacan, M. Özacar, *Renewable Energy*, 2022, **195**, 107-120.

7 R. Zhu, R. Yang, L. Hu, B. Chen, *INT J HYDROGEN ENERG*, 2019, **44**, 25119-25128.

8 Z. Qiao, W. Wang, N. Liu, H.-T. Huang, L. Karuppasamy, H.-J. Yang, C.-H. Liu and J.J. Wu, *INT J HYDROGEN ENERG*, 2021, DOI: 10.1016/j.ijhydene.2021.10.021.

9 L.-L. Dang, T.-T. Zhang, T.-T. Li, T. Chen, Y. Zhao, C.-C. Zhao and L.-F. Ma, *Molecules*, 2022, **27**, DOI: 10.3390/molecules27061917.

10 Y. Geng, X. Zou, Y. Lu, L. Wang, *INT J HYDROGEN ENERG*, 2022, **47**, 11520-11527.

11 Q. Zhang, J. Zhang, L. Zhang, F. Yang, L. Li, and W-L Dai, *Catal. Sci. Technol.*, 2020, **10**, 1030-1039

12 S. Tao, W. Zhong, Y. Chen, F. Chen, P. Wang and H. Yu, *Catal. Sci. Technol.*, 2022, DOI: 10.1039/D2CY01315K.

13 W. Huang, Z. Li, C. Wu, H. Zhang, J. Sun, Q. Li, *J Mater Sci Technol*, 2022, **120**, 89-98.

14 P. Xue, X. Pan, J. Huang, Y. Gao, W. Guo, J. Li, M. Tang and Z. Wang, *ACS Appl. Mater*,

2021, **13**, 59915-59924.